Synthesis and giant dielectric behavior of $CaCu_3Ti_4O_{12}$ ceramics prepared by polymerized complex method

Chivalrat Masingboon[a], Prasit Thongbai[a], Santi Maensiri[a,*],
Teerapon Yamwong[b], Supapan Seraphin[c]

[a] Integrated Nanotechnology Research Center (INRC) and Small & Strong Materials Group (SSMG), Department of Physics,
Faculty of Science, Khon Kaen University, Khon Kaen 40002, Thailand
[b] National Metals and Materials Technology Center (MTEC), Thailand Science Park, Pathumthani 12120, Thailand
[c] Department of Materials Science and Engineering, The University of Arizona, Tucson, AZ 85721, USA

Abstract

Nano-sized powders of $CaCu_3Ti_4O_{12}$ were synthesized by a polymerized complex method and calcined at 600, 700 and 800 °C in air for 8 h. The diameter of the powders ranges from 30 to 100 nm. The $CaCu_3Ti_4O_{12}$ powders were characterized by TG-DTA, XRD, FTIR, SEM and TEM. Sintering of the powders was conducted in air at 1100 °C for 16 h. The XRD results indicated that all sintered samples have a typical perovskite $CaCu_3Ti_4O_{12}$ structure with some amount of $CaTiO_3$ and CuO. SEM micrographs of the sintered $CaCu_3Ti_4O_{12}$ ceramics showed the average grain size of 10–15 μm. The samples exhibit a giant dielectric constant, ε' of 10,000–20,000. It is found that ε is independent on the frequency and weakly dependent on temperature. The Maxwell–Wagner polarization mechanism is used to explain the high permittivity in these ceramics. It is also found that all three sintered samples have the same activation energy of grains, which is 0.116 eV. On the other hand, the activation energy of grain boundaries is found to be 0.219, 0.391 and 0.641 eV for $CaCu_3Ti_4O_{12}$ ceramics prepared using the $CaCu_3Ti_4O_{12}$ powders calcined at 600, 700 and 800 °C, respectively.
© 2007 Elsevier B.V. All rights reserved.

Keywords: Powder processing; Electron diffraction; Scanning electron microscopy; X-ray diffraction (XRD); Dielectrics

1. Introduction

Dielectric materials with high dielectric constant, good thermal stability and Ba/Pb-free have particularly attracted ever-increasing attention for their practical applications in microelectronics such as capacitors and memory devices. Recently, there has been a great interest in synthesis and characterization of a perovskite-type compound, calcium copper titanate ($CaCu_3Ti_4O_{12}$, commonly called CCTO) [1–14]. This non-ferroelectric material, unlike commonly used ferroelectrics, exhibits giant dielectric constant of $\varepsilon' \sim 10^4$ for polycrystalline ceramics [1,2] and $\varepsilon' \sim 10^5$ (for single crystals) [3] in the kilohertz region over a large temperature range (from 100 to 600 K). This material does not undergo any structural change over the same temperature range although its dielectric constant abruptly decreases to less than 100 below 100 K, showing a Debye-like relaxation [13]. In addition to its interesting dielectric property, $CaCu_3Ti_4O_{12}$ has remarkably strong linear current–voltage characteristics without the addition of dopants [15]. These excellent properties render this material particularly attractive for a wide range of applications.

So far, several explanations for the origin of the colossal dielectric property of $CaCu_3Ti_4O_{12}$ material have been proposed to be due to either intrinsic or extrinsic effect. Since the giant dielectric response of this material was found to be very sensitive to the microstructure (such as grain size) and processing conditions (such as sintering temperature and time, cooling rate and partial pressure) [11–13,16,17], more investigations tend to believe that the high dielectric constant originates from the extrinsic effect such as internal barrier layer capacitor (IBLC) [11,16], contact-electrode effect [18,19], and special inhomogenity of local dielectric response [20]. Although still unclear, the IBLC explanation of extrinsic mechanism is widely accepted at the present stage [21–26].

* Corresponding author. Tel.: +66 43 202222–9x2248; fax: +66 43 202374.
  E-mail addresses: sanmae@kku.ac.th, santimaensiri@gmail.com
(S. Maensiri).

CCTO was generally prepared by a standard solid-state reaction method [1–3]. This method requires tedious work and a high temperature in the powder preparation process. Moreover, it suffers from the disadvantages of inhomogeneity. In contrast, synthesis from a solution affords the reaction with a homogeneous mixing of the metal ions at the atomic scale, shorter reaction time and at lower temperature [13]. However, it has been only a few reports on the solution methods to synthesize CCTO [8,10,13].

In this paper, we report the synthesis and giant dielectric properties of CCTO prepared by polymerized complex (PC) method. The PC method is a chemical solution process, which has received considerable attention due to its relative simplicity and usefulness for obtaining a homogeneous and fine powder precursor. The synthesized fine CCTO powders were characterized by thermogravimetric and differential thermal analysis (TG-DTA), X-ray diffraction (XRD), Fourier-transform infared (FT-IR) spectroscopy, scanning electron microscopy (SEM) and transmission electron microscopy (TEM). The effects of particle size of the synthesized powders on microstructure and giant dielectric behavior of the sintered CCTO were also investigated.

2. Experimental procedure

The nano-sized powders of the CCTO were prepared by a simple modified sol–gel method. The PC method was first developed by Pechini [27] and has been used to synthesize polycations oxides powders [28–35]. It is based on metallic citrate polymerization with the use of ethylene glycol. A hydrocarboxylic acid, such as citric acid, is used to chelate cations in aqueous solution. The addition of a glycol, such as ethylene glycol, leads to organic ester formation. Polymerization, promoted by heating the mixture, results in a homogeneous resin in which metal ions are uniformly distributed throughout the organic matrix. To prepare the CCTO powders, citric acid (99.7% purity, BDH, England) was first dissolved in ethylene glycol (99.5% purity, Carlo Erba Reacgenti, Italy) by heating and stirring at 80 °C. Subsequently, $Ca(NO_3)_2 \cdot 4H_2O$ (99.9% purity, Kento, Japan), $Cu(NO_3)_2 \cdot 4H_2O$ (99.5% purity, Carlo Erba Reacgenti, Italy) and 75 wt% titanium(diisoproproxide) bis(2,4-pentanedionate) in 2-propanol (99%, Acros organics, USA) in a mole ratio corresponding to the nominal composition of $CaCu_3Ti_4O_{12}$. Citric acid and ethylene glycol were mixed in the respective proportions of 4 and 16 moles for each mole of metal cation. The transparent blue-colored mixture was then stirred at 280 °C until the formation of the dark blue-colored polymer between ethylene glycol and metal citrate complexes was promoted (for about 10 h). As the colloidal solution was condensed, it became highly viscous. This viscous polymeric product was decomposed to a dark mass precursor at 350 °C for several hours in air. This black-solid mass precursor was ground, passed through 106 μm sieve (Test sieve, Endecotts Limited, England) and each separate portion calcined at 600, 700 and 800 °C for 8 h in air. The calcined powder precursors were reground and passed through 106 μm sieve again to break up large agglomerates. The final products were black powders. The prepared CCTO powers were characterized by TG-DTA (Pyris Diamond TG/DTA, PerkinElmer Instrument, USA), X-ray diffraction (PW3040 Philips X-ray diffractometer with Cu Kα radiation (λ = 0.15406 nm), The Netherlands), Fourier transform infrared spectrometer (Spectrum One FT-IR Spectrometer, PerkinElmer Instruments, USA), scanning electron microscopy (LEO SEM VP1450, UK) and transmission electron microscopy (TEM, Hitachi H8100 200 kV). The sieved powders were pressed uni-axially in a 16 mm die with an applied pressure of 100 MPa. The compacts were pressureless-sintered at 1100 °C for 16 h in air in a box furnace, heating and cooling rates of 5 °C min^{-1}. The sintered disc samples of ∼11 mm in diameter with a thickness of ∼2 mm were obtained. The average grain size of each sintered CCTO ceramic was measured using a standard line intercept technique from SEM micrographs of sintered CCTO surfaces and counting at least 200 intercepts for each micrograph. Throughout this article, we assigned symbols of CCTO_PC600, CCTO_PC700
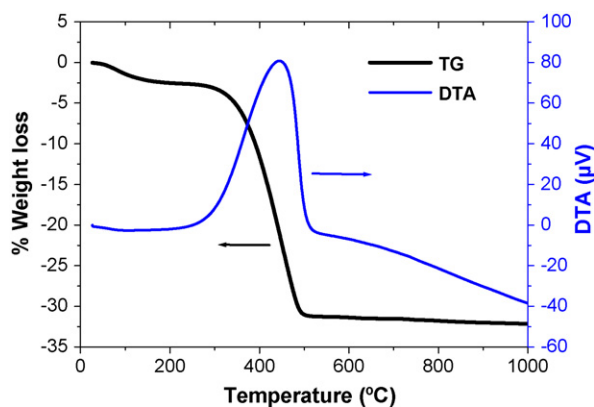

Fig. 1. The TG-DTA curves of the thermal decomposition of CCTO precursor at a heating rate of 15 °C min^{-1} in static air.

and CCTO_PC800 for the CCTO bulk samples fabricated using the powders calcined at 600, 700 and 800 °C, sintered in air at 1100 °C for 16 h, respectively.

The capacitance, C, and loss tangent, tan δ, were carried out as a function of frequency (100 Hz–1 MHz) and temperature (−50 °C to −200 °C), using a Hewlett Packard 4194A Impedance Gain Phase Analyzer at an oscillation voltage of 1 V. Each measured temperature was kept constant with an accuracy of ±1 °C.

The complex permittivity, ε*, was calculated as follows:

$$\varepsilon^* = \varepsilon' - i\varepsilon'' \tag{1}$$

where

$$\varepsilon' = \frac{Cd}{\varepsilon_0 A} \tag{2}$$

$$\varepsilon'' = \varepsilon' \tan \delta \tag{3}$$

where ε_0 is the permittivity in free space, A is the sample area and d is the sample thickness.

3. Results and discussion

Fig. 1 shows the thermal analysis, TG-DTA curves of the powder precursor of CCTO firing with a heating rate of 15 °C min^{-1} in static air from room temperature to 1000 °C. The TG curve shows a major weight loss from 300 to ∼500 °C; no further weight loss was observed up to 1000 °C. The weight loss is related to the combustion of organic matrix. The clear plateau formed between 500 and 1000 °C on the TG curve indicates the formation of CCTO as decomposition product, as confirmed by XRD analysis (discuss in detail later). On the DTA curve, a main exothermic effect were observed between 300 and 500 °C with maxima at 450 °C, indicating that the thermal events was associated with the burnout of organic species involved in the precursor powders (organic mass remained from citric acid and ethylene glycol), of the residual carbon or due to direct crystallization of CCTO from the amorphous component. No further weight loss and no thermal effect were observed above 500 °C, indicating that no decomposition occurs above this temperature. Note that these precursors were calcined in air at 600, 700 and 800 °C for 8 h.

Fig. 2 shows XRD patterns of CCTO powders after calcination in air at (a) 600 °C, (b) 700 °C and (c) 800 °C for 8 h. The main peaks of all calcined CCTO powders are compara-
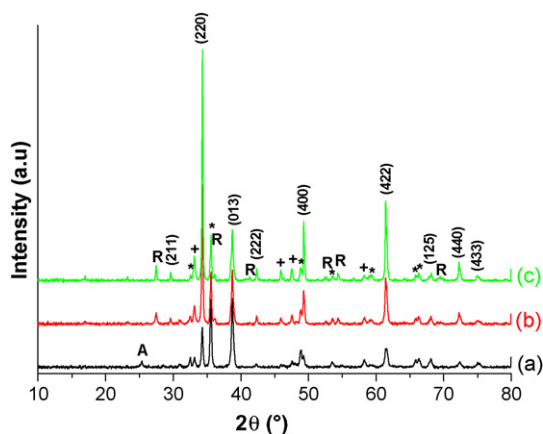
Fig. 2. XRD patterns of CCTO powders calcined for 8 h in air at (a) 600 °C, (b) 700 °C and (c) 800 °C, respectively. +CaTiO$_3$, *CuO, A Anatese TiO$_2$ and R Rutile TiO$_2$.

Fig. 3. FT-IR spectra of CCTO powders calcined for 8 h in air at (a) 600 °C, (b) 700 °C and (c) 800 °C, respectively.

ble to those of the standard powder XRD pattern of CCTO in the JCPDS card No. 75-2188. In addition, the following phases of CaTiO$_3$ (JCPDS card No. 82-0228), CuO (JCPDS card No. 80-0076), Anateses-TiO$_2$ (JCPDS card No. 78-2486) and Rutile-TiO$_2$ (JCPDS card No. 87-0920) were also observed. It is suggested by Guilleemet-Fritsch et al. [36] that the pure CCTO phase is obtained only when the ratio of calcium, copper and titanium are close to the stoichiometric ones. The CaTiO$_3$ and TiO$_2$ phase appear if an excess of titanium is present. It is the excess of titanium that leads to the precipitation of CaTiO$_3$ and TiO$_2$, even if there is no excess of calcium [36]. The formation of CaTiO$_3$ may also cause the excess of Cu with respect with the stoichiometry of CCTO. As a result, the precipitation of the CuO is observed. From the line broadening of the main peaks, the crystallite size (D) was estimated using the Scherrer formula [37]:

$$D = \frac{K\lambda}{(\beta \cos \theta)} \tag{4}$$

where λ is the wavelength of the X-ray radiation, K is a constant taken as 0.9, θ is the diffraction angle. β is the full width at haft maximum (FWHM) and is given by $\beta = (\beta_o^2 - \beta_i^2)^{1/2}$, where β_o and β_i are the widths from the observed X-ray peak and the width due to instrumental effects, respectively. The particle sizes are found to be 43.8 ± 15.6, 55.4 ± 20.1 and 70.9 ± 22.6 nm for the powders calcined at 600, 700 and 800 °C, respectively.

Fig. 3 shows FT-IR spectra of CCTO powders after calcination in air at 600, 700 and 800 °C for 8 h. All three samples show the main absorption bands at 561, 516 and 437 cm^{-1}. These bands are assigned to the absorption regions for Ti ion, which are associated to ν_{Ti-O} of 653–550 cm^{-1} and $\nu_{Ti-O-Ti}$ of 495–436 cm^{-1} [4].

Morphology and microstructure of the calcined CCTO powders and sintered CCTO ceramic samples revealed by SEM are shown in Fig. 4. Fig. 4(a)–(c) shows CCTO particles with sizes of about 50, 80 and 100 nm for the 600, 700 and 800 °C calcined samples, respectively. These values were larger than those obtained from X-ray line broadening calculation. Some agglomerates were observed in all of the calcined powders.
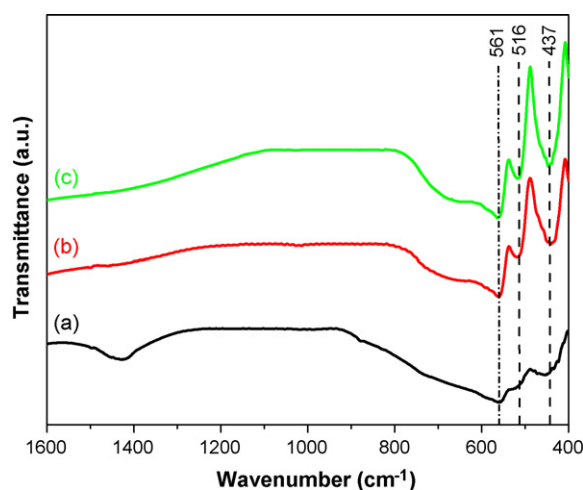
The particle size of the powder increased with increasing calcination temperature. After sintering at 1100 °C for 16 h, the bulk CCTO ceramics with different microstructure were obtained. The CCTO_600 (Fig. 4(d)), CCTO_700 (Fig. 4(e)) and CCTO_800 (Fig. 4(f)) showed a mean grain size of 11.9 ± 4.0 μm, 14.8 ± 6.2 μm and 10.8 ± 4.5 μm, respectively.

Fig. 5 shows TEM images and the corresponding selected area electron diffraction (SAED) patterns of the calcined CCTO powders. It is clearly seen from the TEM bright-field images that all of the samples are consist of nanocrystalline CCTO particles, whose size increases with increasing calcination temperature. The 600 °C calcined sample contains nanoparticles of 30.9 ± 7.8 nm in size whereas the 700 °C calcined sample contains nanoparticles of 58.7 ± 45.4 nm. As expected, the 800 °C calcined sample consists of nanoparticles with the largest particle sizes of 85.3 ± 39.9 nm. It is noted that the particle sizes observed by TEM are not in agreement with results determined by XRD and SEM (see Table 1). The error in the particle sizes obtained from the XRD results is large, and the average values obtained from SEM are significantly larger than that obtained from XRD. These differences could be resulted from some dispersion or inhomogeneity in the particles size of the samples. Electron diffraction of particles with higher calcination temperature contains more intense spots as shown in the 700 and 800 °C calcined powders, indicating the larger particle size of highly crystalline compared to the 600 °C calcined samples. The interplanar spacings (d_{hkl}) measured from the selected-area electron diffraction patterns are in good agreement with the values

Table 1
Summary of particle size analysis obtained from XRD and TEM; and lattice parameter (from XRD) of CCTO powders compared to the ASTM value

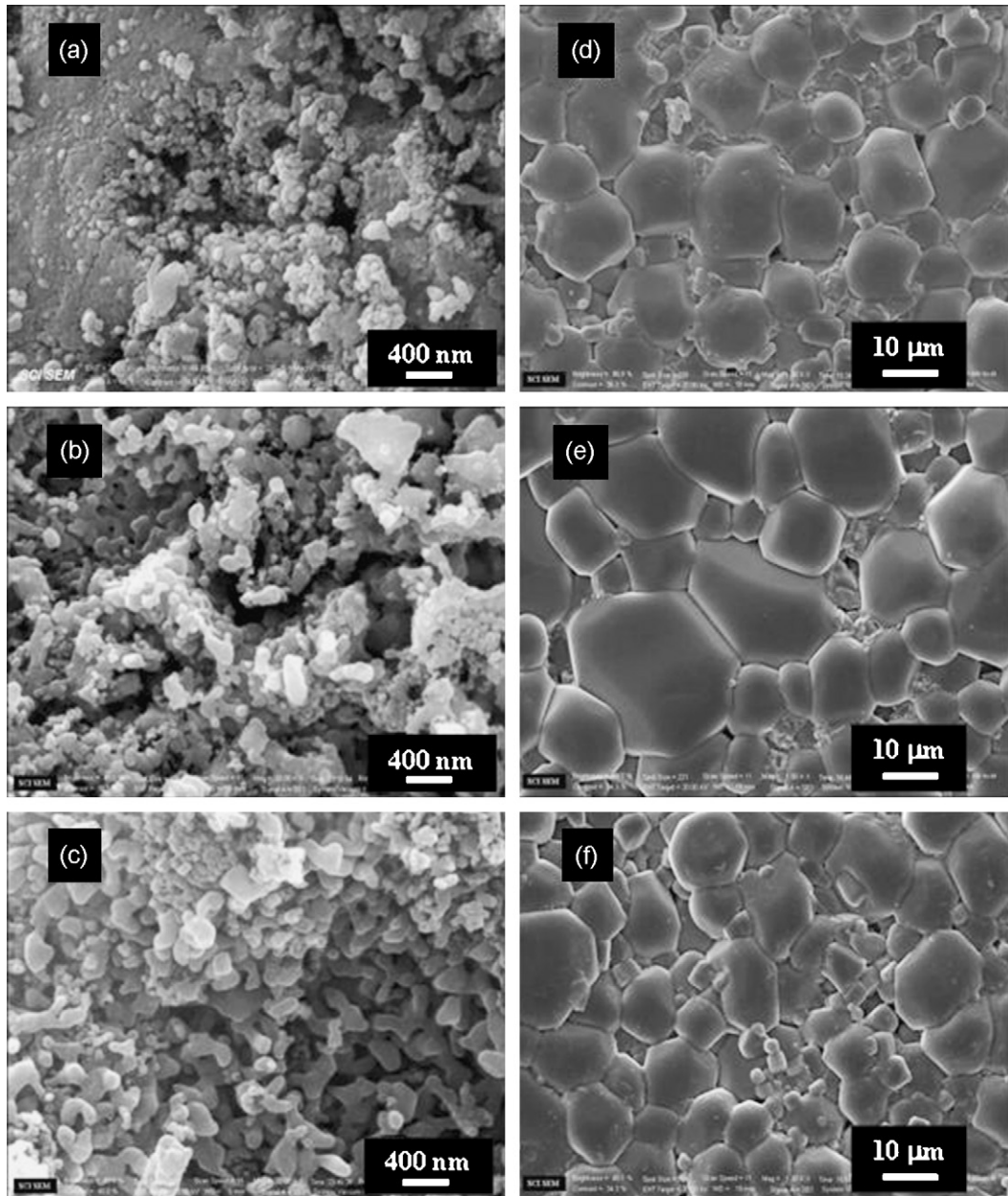| Material	Particle size from XRD (nm)	Particle size from TEM (nm)	Lattice parameter a (Å)
ASTM (75-2188)	–	–	7.391 ± 0.001
600 °C powders	43.8 ± 15.6	30.9 ± 7.8	7.374 ± 0.002
700 °C powders	55.4 ± 20.1	58.7 ± 45.4	7.389 ± 0.001
800 °C powders	70.9 ± 22.6	85.3 ± 39.9	7.398 ± 0.002

Fig. 4. SEM micrographs of the CCTO powders and sintered CCTO materials. (a)–(c) are the powders calcined for 8 h in air at 600, 700 and 800 °C, respectively. (d)–(f) are the microstructure of the sintering CCTO_PC600, CCTO_PC700 and CCTO_PC800, respectively.

obtained from the standard data JCPDS: 75-2188 (for CCTO) and 89-0056 (for $CaTiO_3$) as summarized in Table 2.

Fig. 6 shows XRD patterns of the CCTO ceramics sintered in air at 1100 °C for 16 h, confirming a single phase of CCTO in all the samples although a small amount of $CaTiO_3$ and CuO were present in all the sintered samples. The presence of additional $CaTiO_3$ in the sintered samples is possibly due to the presence of excess titanium as suggested Guilleemet-Fritsch et al. [36]. Therefore, we think that the excess of titanium leads to the precipitation of $CaTiO_3$ in our sintered samples. For the presence of the CuO phase, it is possible that the Cu rich phase derives from the diffusion of Cu to the defects present, after which gross excess causes the crystallization of the separate CuO phase [38]. The CuO phase within the ceramics implies that excess copper is in the form of a copper rich phase at the grain boundaries [38,39]. However, further work on careful investigation of the stoichiometry of the CCTO ceramics using energy dispersive spectroscopy (EDS) is needed to confirm the Ca/Cu/Ti cationic ratio in our CCTO ceramics.

Fig. 7 shows the frequency dependence of the ε' and ε'' of the sintered CCTO ceramics (CCTO_PC600, CCTO_PC700 and CCTO_PC800) at various temperature between −50 and −10 °C. Fig. 7(a.1)–(c.1) shows that the CCTO ceramics (CCTO_PC600, CCTO_PC700 and CCTO_PC800) have very high dielectric constant, ε', of 10000–20000 at 1 kHz. ε' has little frequency dependence at low frequency (below 100 kHz). The high ε' at low frequency may possibly be a contribution from grain boundary in these sintered CCTO ceramics [40]. The val-
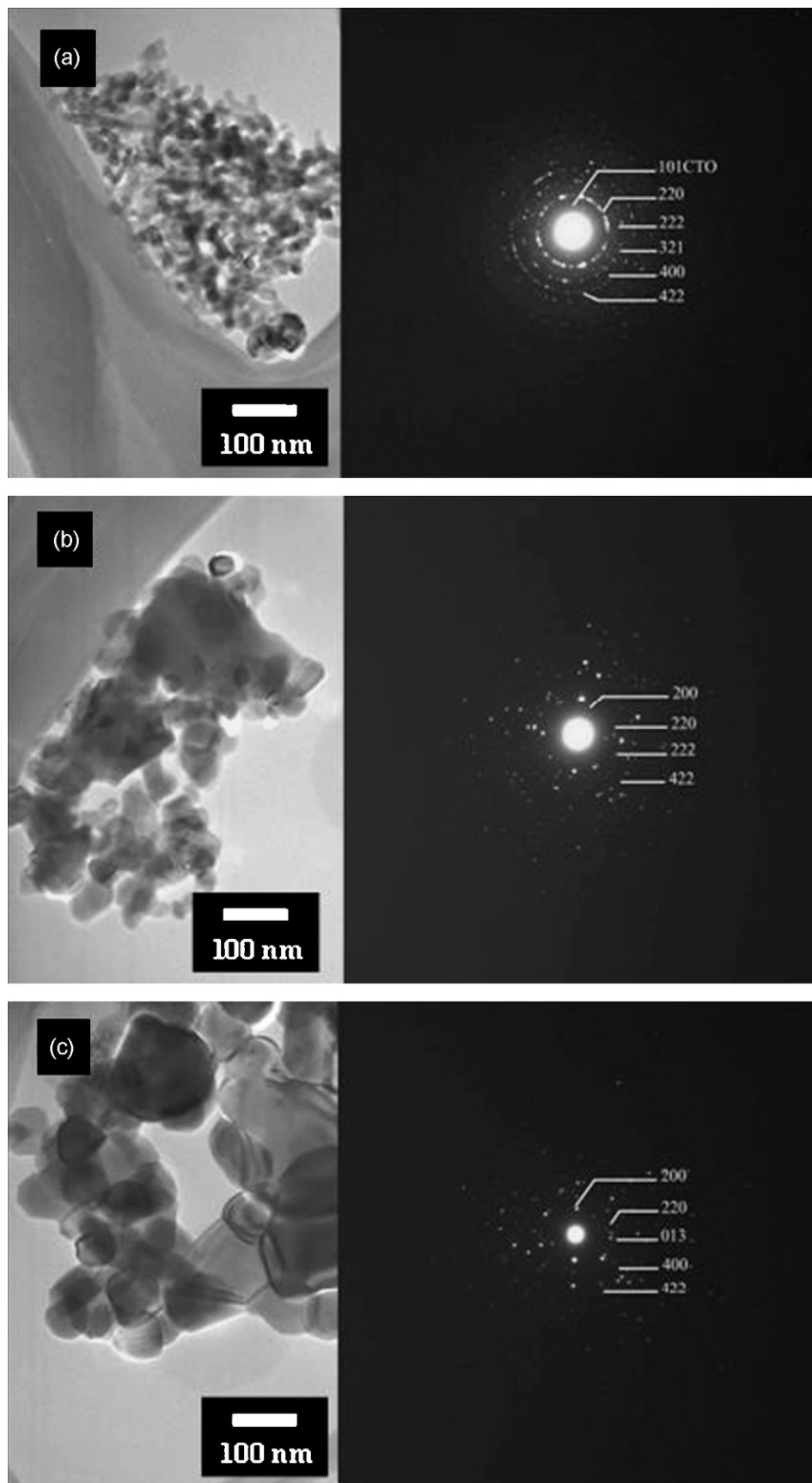
Fig. 5. Bright field TEM images with corresponding selected-area electron diffraction (SAED) patterns of CCTO powders calcined in air for 8 h: (a) 600 °C; (b) 700 °C; (c) 800 °C, respectively. 101CTO stands for (1 0 1) plane of CaTiO$_3$.

Table 2
Measured interplanar spacings (d_{hkl}) obtained from selected-area electron diffraction patterns of CCTO samples calcined at 600, 700 and 800 °C for 8 h shown in Fig. 5

Ring	Measured interplanar spacing of CCTO samples d_{hkl} (Å)			Standard data (JCPDS: 75-2188)	
	600 °C powder	700 °C powder	800 °C powder	d_{hkl} (Å)	hkl
R_1	–	3.5735	3.5735	3.6955	200
R_2	2.6703	2.6413	2.6557	2.6131	220
R_3	–	–	2.3143	2.3372	013
R_4	2.1696	2.1504	–	2.1336	222
R_5	1.9597	–	–	1.9753	321
R_6	1.7802	–	1.7868	1.8477	400
R_7	1.567	1.5379	1.5527	1.5086	422

Corresponding values from the standard data JCPDS: 75-2188 are also provided for a comparison.

ues are similar to the those reported by Jin et al. [10] and Liu et al. [13], who reported values of $\varepsilon' \sim 10^4$ (at 1 kHz) for samples prepared from a solution route; and by Ramirez et al. [1] and Bender and Pan [12], whose samples prepared from a solid-state reaction method. These values, however, are much higher than 3000 of the sol–gel synthesized CCTO ceramics reported by Jha et al. [8].

The frequency dependence of the observed dielectric relaxation, ε'', shown in Fig. 7(a.2)–(c.2). By considering these results, we cannot apply the empirical Cole–Cole relation to fit these data because at low frequency the samples contain numerous grain boundaries or grain boundaries relaxation [40]. However, we can apply the Debye-like relaxation peak due to the presence of the grains. The ε'' shows a clear Debye-like relaxation peak shifting from a constant value at low frequency to a small saturated value at higher frequency. The electrical response from grains has a very high response frequency because of their small resistance and capacitance [13]. We can determine the dielectric relaxation time, τ, also by following the Arrhenius law of

$$\tau = \tau_0 \exp\left(\frac{U}{k_B T}\right) \tag{5}$$

where τ_0 is the pre-exponential factor, U is the activation energy for the relaxation, k_B is the Boltzmann constant and T is the absolute temperature. Fig. 8 illustrates the relationship of τ and T for all three CCTO samples. The activation energy of an electrical response, at different temperature can be derived from the response time ($\tau = 1/2\pi f$, where f is the response frequency at which the imaginary part of the complex impedance has a maximum). From the fitting (Fig. 8), we obtain the activation energy of the dielectric relaxation for CCTO_PC600, CCTO_PC700 and CCTO_PC800 to be of the same value of 0.116 eV.

Fig. 9 shows the fit of the ε'' of the CCTO ceramics (CCTO_PC600, CCTO_PC700 and CCTO_PC800) to equation [41]

$$\varepsilon'' \approx \frac{\sigma_{dc}}{\varepsilon_0 \omega} \tag{6}$$

where σ_{dc} is conductivity at low frequency at various temperature between 160 and 200 °C. As expected, at high temperature and low frequency, the ε'' is increased mainly due to the increase of the dc conductivity [34,42]. From the fitted results, we can obtain the dc conductivity for the CCTO ceramics at different temperatures and then we can fit σ_{dc} also by following the Arrhenius law of

$$\sigma_{dc} = \sigma_{dc}^0 \exp\left(\frac{U_{dc}}{k_B T}\right) \tag{7}$$

where σ_{dc}^0 is the pre-exponential factor, U_{dc} is the activation energy for the dc conductivity. The correlation of these values is shown in Fig. 10. From the fitting, we obtain the activation energy of the dielectric relaxation for CCTO_PC600, CCTO_PC700 and CCTO_PC800 to be 0.219, 0.391 and 0.647 eV, respectively. These values are close to the activation energy of the grain boundaries reported earlier in the literature for the CCTO, 0.24 [9], 0.34 [26] and 0.60 eV [11]. Our results support the hypothesis of the existence of internal barrier layers between the grains. In other words, our results indicate that the behavior of ε'' at low frequency (in Fig. 7) is a result of the grain boundaries barrier.
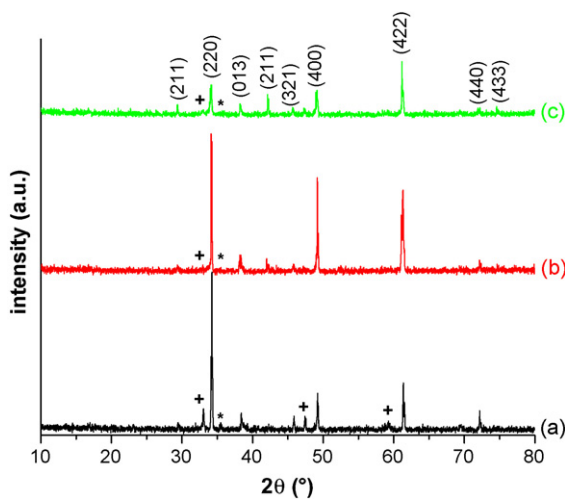

Fig. 6. XRD patterns of (a) 600 °C, (b) 700 °C and (c) 800 °C, respectively. All sintering was done in air at 1100 °C for 16 h. The indexed planes indicated in (c) pattern are for CCTO main structure. +CaTiO$_3$ and * CuO.
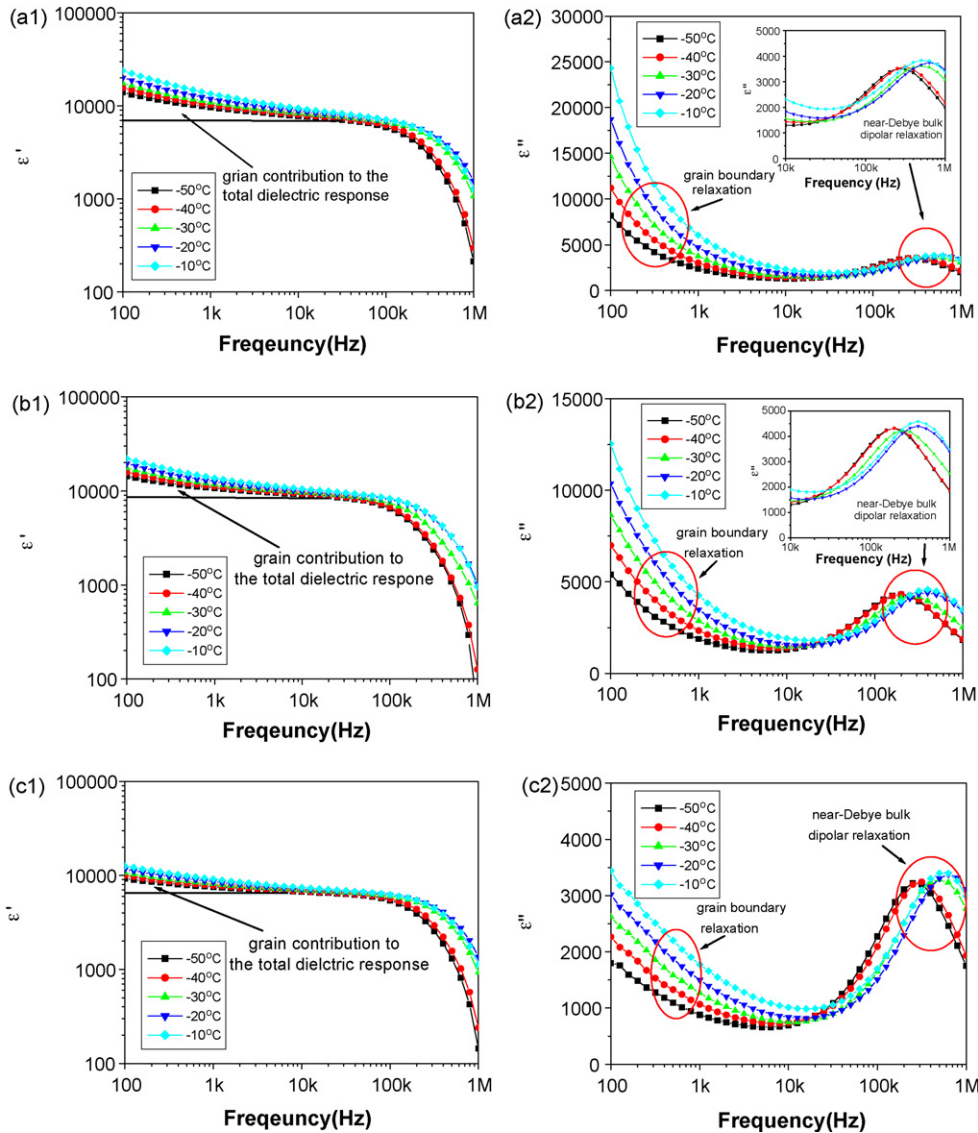
Fig. 7. The frequency dependence of the complex permittivity, ε^*, at low temperature between -50 and $-10\,^{\circ}$C for (a.1)–(a.2) CCTO_PC600, (b.1)–(b.2) CCTO_PC700 and (c.1)–(c.2) CCTO_PC800, respectively. (a.1)–(c.1) display the real part ε'; (a.2)–(c.2) display the imaginary part ε''.
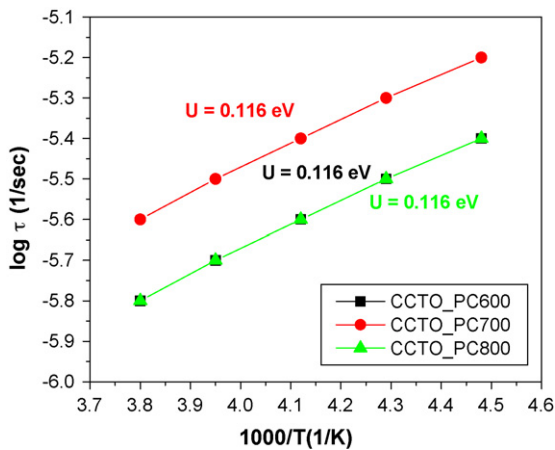

Fig. 8. Arrhenius plot of dielectric relaxation time τ for the three sintered samples.

To interpret the dielectric in the CCTO ceramics, the Maxwell–Wagner relaxation was used to describe a series array of two sub-circuits, one in the grain and the other at the grain boundaries [13,43]. In each sub-circuit, the resistor and capacitor are in parallel. In this circuit, we can present the static-permittivity, ε'_s, and dielectric relaxation time, τ, in the following form

$$\varepsilon'_s = \frac{R_g^2 C_g + R_{gb}^2 C_{gb}}{C_0(R_g + R_{gb})^2} \tag{8}$$

$$\tau = \frac{R_g R_{gb}(C_g + C_{gb})}{R_g + R_{gb}} \tag{9}$$

where C_g and C_{gb} are the capacitance of grain and grain boundaries, respectively; R_g and R_{gb} are the resistor of grain and grain boundaries, respectively; C_0 is the empty cell constant and τ is the time constant.
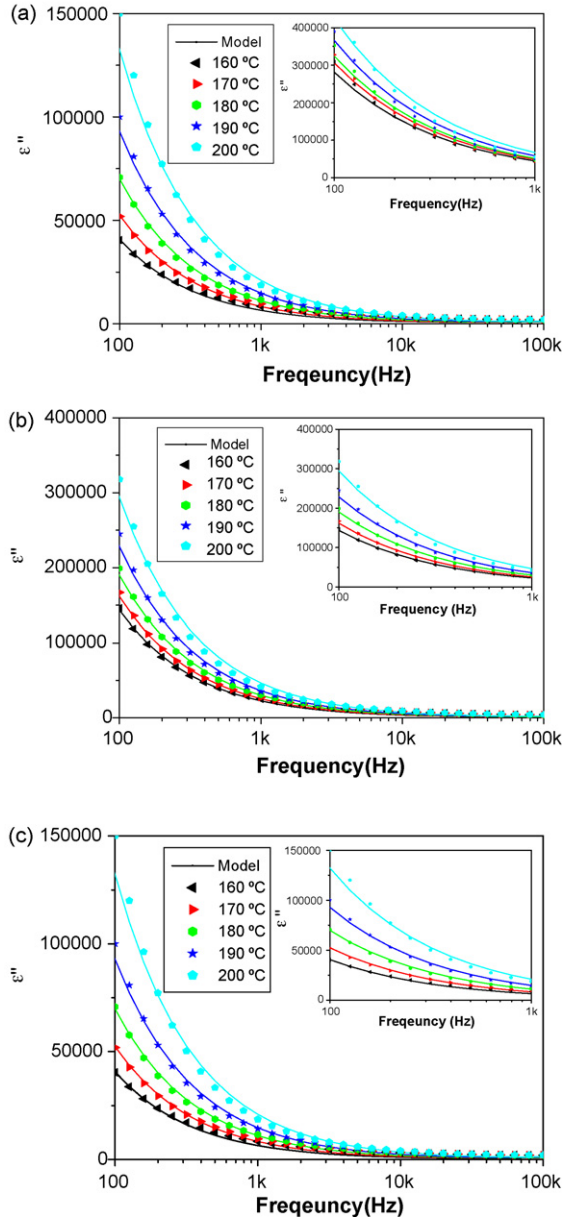
Fig. 10. Arrhenius plot of dc conductivity σ_{dc} for the three sintered samples.

Fig. 9. The frequency dependence of the dielectric loss ε'' at high temperature ranging between 160 and 200 °C for (a) CCTO_PC600, (b) CCTO_PC700 and (c) CCTO_PC800, respectively. The solid lines are the fits according to Eq. (6).

It has been reported in the literature that for CCTO, $R_{gb} \gg R_g$ and $C_{gb} \approx 10\,C_g$ [13,43]. We can estimate the static-permittivity ε'_s from Eq. (8),

$$\varepsilon'_s \approx \frac{C_{gb}}{C_0} \tag{10}$$

Thus, ε'_s is determined by the ratio between grain boundary capacitance, C_{gb}, and empty cell capacitance, C_0. Hence ε'_s is constant when C_{gb} is temperature and frequency independent. The implication is in good agreement with our experimental results. We observed that dielectric constant is not dependent on the frequency and only weakly dependent on the temperature.
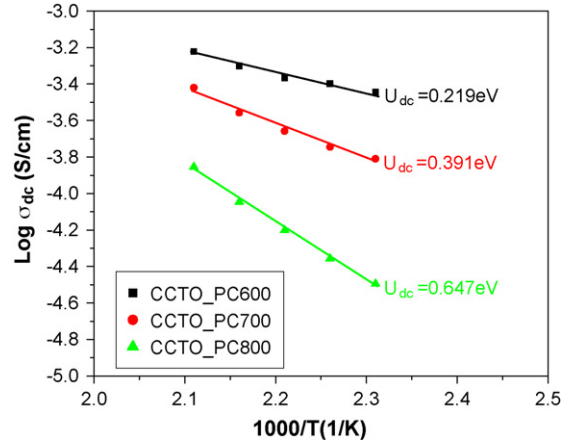
If we assumed that the grain boundary form a two-layer capacitor with a thickness of $(d_g + d_{gb})$, where d_g and d_{gb} are the thickness of the grain and the grain boundary layer, respectively, from Eq. (10), one obtains $\varepsilon'_s \approx \varepsilon_{gb}(d_g + d_{gb})/d_{gb}$; here ε_{gb} is the dielectric constant of the grain boundary layer. Therefore, even a small dielectric constant ε_{gb} can lead to a giant dielectric constant ε'_s if the ratio $(d_g + d_{gb})/d_{gb}$ is large. If the grain is about 10 μm, the grain boundary layer is about 0.01 μm and $\varepsilon_{gb} = 10$, then $\varepsilon'_s \approx 10,000$. Therefore, the Maxwell–Wagner relaxation can be used to explain the giant dielectric constant of our CCTO samples.

Using the conditions, $R_{gb} \gg R_g$ and $C_{gb} \approx 10\,C_g$ [13,43]. We can approximately obtain the time constant, τ, from Eq. (9),

$$\tau \approx R_g C_{gb} = (R_g C_g)\frac{C_{gb}}{C_g} = \tau_g \frac{C_{gb}}{C_g} \tag{11}$$

where $\tau_g = R_g C_g$ is the response time of the grain. It has been reported that C_g and C_{gb} are independent of temperature [11,43], thus, we can deduce τ_g that follows the Arrhenius law, Eq. (5). Let $\tau_g = \tau_g^0 \exp(U_g/k_B T)$ (τ_g^0 is pre-exponential factor and U_g is the activation energy of the grain conduction process), then we modify Eq. (11) to

$$\tau \approx R_g C_{gb} = \frac{C_{gb}}{C_g}\left(\tau_g^0 \exp\left(\frac{U_g}{k_B T}\right)\right) \tag{12}$$

From Eq. (12), τ and τ_0 have the same temperature dependence and the electrical response of the grains has the same activation energy as that of the observed dielectric relaxation. Thus, we can conclude that the activation energy for the response of the grains in CCTO_PC600, CCTO_PC700 and CCTO_PC800 are 0.116 eV, which are close to the values of 0.109 eV for a chemical solution synthesized CCTO and 0.112 eV for the recently reported by our group [14]. However, the value of 0.116 eV is lager than 0.08 eV, which was reported for samples made by solid-state reaction [11]. The activation energy of grain in CCTO_PC600, CCTO_PC700 and CCTO_PC800 are lager than activation energy of grain in sample made by solid-state reaction, which may imply that there are fewer oxygen vacancies in the grains of CCTO_PC600,

CCTO_PC700 and CCTO_PC800. This is reasonable because CCTO_PC600, CCTO_PC700 and CCTO_PC800 were sintered from powders. These powders were calcined at low temperature (600, 700 and 800 °C) compared to the temperature needed for the solid-state processing, which calcined at 1000 °C [11]. Similar suggestion was explained by Liu et al. [13].

4. Conclusions

Nanocrystalline $CaCu_3Ti_4O_{12}$ powders with particle sizes of 30–100 nm have been synthesized by the polymerized complex route. The powders were used to prepared bulk CCTO ceramics, which exhibit giant dielectric response and have the dielectric constant as high as 10,000–20,000 at 1 kHz. The dielectric constant is weakly temperature dependent over the temperature range of −50 °C to 200 °C. The high dielectric-constant responses of these CCTO ceramics are not attributed to the ferroelectric behavior, but rather to the Maxwell–Wagner polarization mechanism.

Acknowledgements

References

[1] A.P. Ramirez, M.A. Subramanian, M. Gardel, G. Blumberg, D. Li, T. Vogt, S.M. Shapiro, Solid State Commun. 115 (2000) 217.
[2] M.A. Subramanian, L. Dong, N. Duan, B.A. Reisner, A.W. Sleight, J. Solid State Chem. 151 (2000) 323.
[3] C.C. Homes, T. Vogt, S.M. Shapiro, S. Wakimoto, A.P. Ramirez, Science 293 (2001) 73.
[4] A.F.L. Almeida, R.S. de Oliveira, J.C. Góes, J.M. Sasaki, A.G. Souza Filho, J. Mendes Filho, A.S.B. Sombra, Mater. Sci. Eng. B 96 (2002) 275.
[5] M.A. Subramanian, A.W. Sleight, Solid State Sci. 4 (2002) 347.
[6] Z. Yu, C. Ang, J. Appl. Phys. 91 (2002) 794.
[7] L. Fang, M.R. Shen, Thin Solid Films 440 (2003) 60.
[8] P. Jha, P. Arora, A.K. Ganguli, Mater. Lett. 57 (2003) 2443.
[9] J. Li, A.W. Sleight, M.A. Subramanian, Solid State Commun. 135 (2005) 260.
[10] S. Jin, H. Xia, Y. Zhang, J. Guo, J. Xu, Mater. Lett. 61 (2007) 1404.
[11] D.C. Sinclair, T.B. Adams, F.D. Morrison, A.R. West, Appl. Phys. Lett. 80 (2002) 2153.
[12] B.A. Bender, M.J. Pan, Mater. Sci. Eng. B 117 (2005) 339.
[13] J. Liu, Y. Sui, C. Duan, W.N. Mei, R.W. Smith, J.R. Hardy, Chem. Mater. 18 (2006) 3878.
[14] P. Thongbai, C. Masingboon, S. Maensiri, T. Yamwong, S. Wongsaenmai, R. Yimnirun, J. Phys. Condens. Matter 19 (2007) 236208.
[15] S. Chung, I. Kim, S. Kang, Nat. Mater. 3 (2006) 774.
[16] T.T. Fang, H.K. Shiau, J. Am. Ceram. Soc. 87 (2004) 2072.
[17] S.F. Shao, J.L. Zhang, P. Zheng, W.L. Zhong, C.L. Wang, J. Appl. Phys. 99 (2006) 084106.
[18] P. Lunkenheimer, V. Bobnar, A.V. Pronin, A.I. Ritus, A.A. Volkov, A. Loidl, Phys. Rev. B 66 (2002) 052105.
[19] P. Lunkenheimer, R. Fichtl, S.G. Ebbinghaus, A. Loidl, Phys. Rev. B 70 (2004) 172102.
[20] M.H. Cohen, J.B. Neaton, L.X. He, D. Vanderbilt, J. Appl. Phys. 94 (2003) 3299.
[21] L. Zhang, Z.J. Tang, Phys. Rev. B 70 (2004) 174306.
[22] A.R. West, T.B. Adams, F.D. Morrison, D.C. Sinclair, J. Eur. Ceram. Soc. 24 (2004) 1439.
[23] G. Chiodeli, V. Massarotti, D. Capsoni, M. Bini, C.B. Azzoni, M.C. Mozzati, P. Lupotto, Solid State Commun. 132 (2004) 241.
[24] D. Capsoni, M. Bini, V. Massarotti, G. Chiodelli, M.C. Mozzatic, C.B. Azzoni, J. Solid State Chem. 177 (2004) 4494.
[25] S.V. Kalinin, J. Shin, G.M. Veith, A.P. Baddorf, M.V. Lobanov, H. Runge, M. Greenblatt, Appl. Phys. Lett. 86 (2005) 102902.
[26] T.T. Fang, L.T. Mei, H.F. Ho, Acta Mater. 54 (2006) 2867.
[27] M.P. Pechini, US Patent 3,330,697, (1967).
[28] P.A. Lessing, Am. Ceram. Soc. Bull. 168 (1989) 1002.
[29] M. Kakihana, J. Sol Gel Sci. Technol. 6 (1996) 7.
[30] M. Kakihana, M. Arima, Y. Nakamura, M. Yashima, M. Yoshimura, Chem. Mater. 11 (1999) 438.
[31] R.A. Rocha, E.N.S. Muccillo, Chem. Mater. 115 (2003) 4268.
[32] M. Vijayakumar, Y. Inaguma, W. Mashiko, M.P. Crosnier-Lopez, C. Bohnke, Chem. Mater. 16 (2004) 2719.
[33] T. Seretawa, V. Amornkitbamrung, T. Burinprakhon, S. Maensiri, Inter. J. Nanosci. 4 (2005) 237.
[34] S. Maensiri, P. Thongbai, T. Yamwong, Acta Mater. 55 (2007) 2851.
[35] K. Wongsaprom, E. Swatsitang, S. Srijaranai, S. Maensiri, S. Seraphin, Appl. Phys. Lett. 90 (2007) 162506.
[36] S. Guillemet-Fritsch, T. Lebey, M. Boulos, B. Durand, J. Eur. Ceram. Soc. 26 (2006) 1245.
[37] B.D. Cullity, S.R. Stock, Elements of X-ray Diffraction, Prentice Hal1, Englewood Cliffs, 2001.
[38] P. Leret, J.F. Fernandez, J. de Frutos, D. Fernández-Hevia, J. Eur. Ceram. Soc. 27 (2007) 3901.
[39] C.K. Yeoh, M.F. Ahmad, Z.A. Ahmad, J. Alloys Compd. 443 (2007) 155.
[40] M.A. Ramirez, P.R. Bueno, J.A. Varela, E. Longo, Appl. Phys. Lett. 89 (2006) 212102.
[41] K.C. Kao, Dielectric Phenomena in Solids, Elsevier Academic Press, London, 2004.
[42] J. Wu, C.W. Nan, Y. Lin, Y. Deng, Phys. Rev. Lett. 89 (2002) 217601.
[43] J. Liu, C.G. Duan, W.G. Yin, W.N. Mei, R.W. Smith, J.R. Hardy, Phys. Rev. B 70 (2004) 144106.